CERN
Summer Student Programme 2021
รายงานการเข้าร่วมโครงการนักศึกษาภาคฤดูร้อน

ระหว่างวันที่ 5 กรกฎาคม - 27 สิงหาคม 2564

นายสิทธา เจียมบุรเศรษฐ

ภาควิชาฟิสิกส์

คณะวิทยาศาสตร์ มหาวิทยาลัยมหิดล

Muon Acceptance through the production straight of nuSTORM Ring

Author: Sittha Jeamburaset (Imperial College London)
Supervisor: Paul Kyberd (Brunel University)

CERN Summer Student Programme 2021

E-mail: sittha.jeamburaset21@imperial.ac.uk

Abstract: In this work, we approximate actual particles of muons captured by the nuSTROM ring as they decay from pion beam. We study the effect of limiting the phase space of muons generated using nuSim, a nuSTORM ring simulation tool. We look at several fundamental aspects of the effect, such as the muon spectrum and the efficiency with which they can be produced per pion. To determine the normalization of the muons per proton, we integrate the data with data from the NuMI target. Then, using this number and a muon decay simulation, we can calculate the total normalization of neutrinos per proton.

Contents

1 Introduction

Neutrino has played the significant role in our understanding of nuclear and particle physics. Studying how neutrinos interact with matter is one of the most important observations since it enhances the precision experiment of neutrino interaction cross-sections in order to reduce statistical error in other experiments and searching for particles beyond the standard model. The energy range considered by current measurements of charged-current neutrino and antineutrino cross sections for the neutrino nucleon interaction is summarized in fig.1 [5].

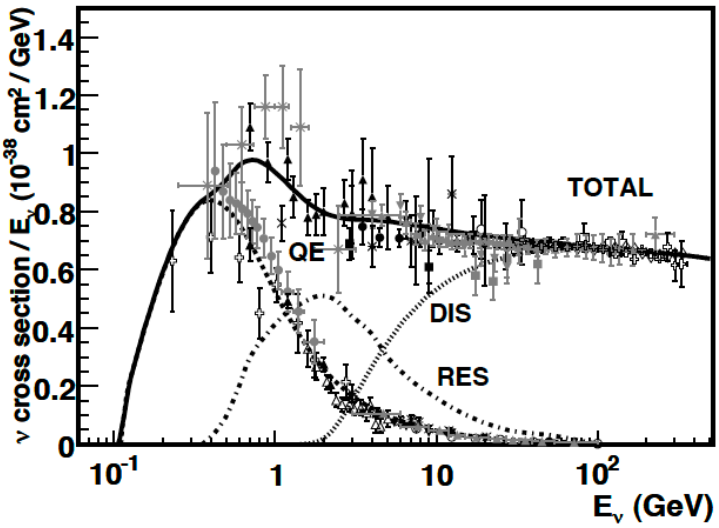

Figure 1: Total neutrino and antineutrino per nucleon CC cross sections (for an isoscalar target) divided by neutrino energy and plotted as a function of energy

nuSTORM, Neutrinos from Stored Muons, is the first neutrino-beam facility aimed to store the muon beam with central momentum ranging from 1 GeV/c to 6 GeV/c. For neutrino energies less than 2 GeV, neutrino-nucleon interactions are dominated by quasi-elastic (QE) process: $\nu_\mu n \to \mu^- p$, $\bar{\nu}_\mu p \to \mu^+ n$ and resonance single pion production which the neutrino interaction produces a baryon resonance $\nu_\mu N \to \mu^-(N^* \to \pi N')$. At higher energies, $E_\nu > 2$ GeV, deep inelastic scattering and multi pion production are of interest.

In this work, we study the muon production of the pion decay by simulating the production straight of the nuSTORM ring with nuSim [1], approximate the muon distribution captured by the nuSTORM ring and evaluate the normalization through the simulation chain.

The paper is organized as follows. In section 2, we look at the basic features of the pion decay and its yield simulated from nuSim. In section 3, we approximate the distribution of the captured muons by limiting their phase space. In section 4, we look at the effect of limiting and calculate the useful characteristics, such as mean energy, width, emittance of the muon beam as well as their normalization.

2 Pion Decay

The magnetic channel is designed to deliver a pion beam with central momentum p_π and momentum spread $10\% p_\pi$ of a parabolic distribution to the muon decay ring. The pion beam is injected into the production straight of the decay ring and then it will decay into muon and muon-neutrino.

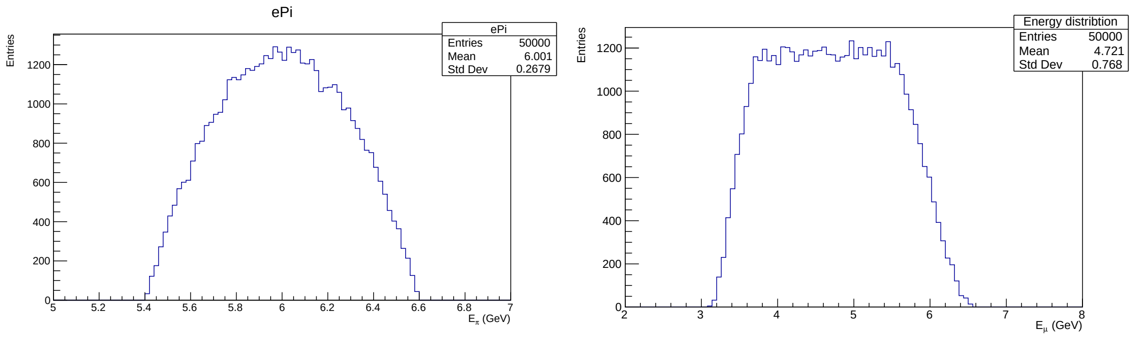

(a) Energy distribution of the pion

(b) Energy distribution of the muon

Figure 2: Energy distribution of the pion generated at 6 GeV with $10\% p_\pi$ and distribution of the muon with a flat top

2.1 Kinematics

For the pion decays, $\pi^\pm \to l^\pm \nu$, with l standing for an e or μ, we concentrate for only μ production since e provide insignificant contribution compared to the μ in this study. We can derive their kinematics by first looking in the pion rest frame and then boost them to the nuSTORM lab frame. Throughout this section units are used in which $\hbar = c = 1$.
In pion rest frame, the muon and neutrino go out back to back after the pion decay $\vec{p_\nu} = -\vec{p_\mu}$. We can write the four momentum of the muon as

$$P_\mu = (E_\mu, p_x, p_y, p_z)$$

For neutrinos, we treat them as massless particles $E_\nu = |\vec{p}|$. Thus, the invariant quantity is

$$P^2 = {m_\mu}^2 = {E_\mu}^2 - |\vec{p}|^2 = {E_\mu}^2 - {E_\nu}^2$$

With $m_\pi = E_\mu + E_\nu$ and $|\vec{p}|^2 = {E_\mu}^2 - {m_\mu}^2$, we have

$$E_\mu = \frac{{m_\pi}^2 + {m_\mu}^2}{2m_\pi} \qquad \text{and} \qquad |\vec{p}| = \frac{{m_\pi}^2 - {m_\mu}^2}{2m_\pi}$$

Four momentum of the muon in spherical coordinate is given by

$$P_\mu = (E_\mu \quad, |\vec{p}|\sin\phi\cos\theta \quad, |\vec{p}|\sin\phi\sin\theta \quad, |\vec{p}|\cos\phi)$$

In Lab frame, when we boost the pions along z-direction, we have

$$p_z{}' = \gamma(p_z + \beta E_\mu) \qquad \text{and} \qquad E_\mu{}' = \gamma(E_\mu + \beta p_z)$$

Where $\gamma = \epsilon/m_\pi$ (ϵ is the beam energy) and $\beta = \sqrt{1 - 1/\gamma^2}$
Finally, the four momentum of the muon is given by

$$P_\mu{}' = (\gamma(E_\mu + \beta|\vec{p}|\text{cos}\phi) \quad , |\vec{p}|\text{sin}\phi\text{cos}\theta \quad , |\vec{p}|\text{sin}\phi\text{sin}\theta \quad , \gamma(|\vec{p}|\text{cos}\phi + \beta E_\mu)) \tag{2.1}$$

Hence, the transverse momentum and the polar angle of the muons when we boost along z-direction are

$$p_T{}' = p_T = |\vec{p}|\text{sin}\phi \qquad \text{and} \qquad \phi' = \text{arctan}\frac{|\vec{p}|\text{sin}\phi}{\gamma(|\vec{p}|\text{cos}\phi + \beta E_\mu)} \tag{2.2}$$

Both are independent of azimuthal angle. They depend on only a polar angle defined in the pion rest frame. We can now utilise these results to determine whether the kinematic limit in our graphs is valid or not.

2.2 p_T Distribution

In pion rest frame, the muons can go to any directions. There is no particular direction. However, when we boost the muons along z-direction, the muons are likely to align around z-axis with the same transverse momentum (p_T) as in the pion rest frame. As a result, in both the pion rest frame and the nuSTORM frame, the transverse momentum distribution is the same as we expect in the equation 2.2.

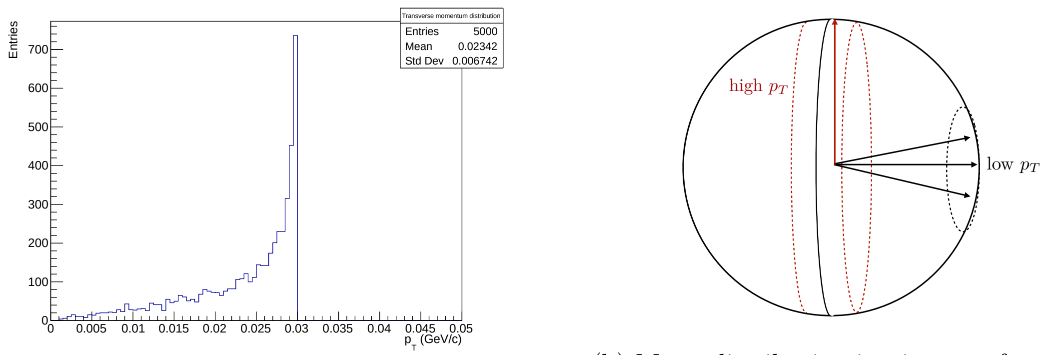

(a) p_T distribution

(b) Muon distribution in pion rest frame

Figure 3

Fig. 3a indicates the distribution of p_T of the muon. As p_T increases, the events get more frequent and eventually come to a halt at 0.03 GeV/c, when the particles align on the $x-y$ plane. Regarding fig.3b, we can see clearly that if the particle momentum distribution is uniform throughout the sphere's surface, the low p_T region has a smaller area than the high p_T region. As a result, the area with high p_T has more events than the area with lower p_T.

2.3 θ and ϕ Distribution

When we boost the muons along z-direction, the muons align around z-axis with some polar angles (ϕ) and the boost has no effect on the components of p_x and p_y. Thus, the azimuthal angle distribution is uniform. However, regarding the polar angle distribution, in fig.4a, the

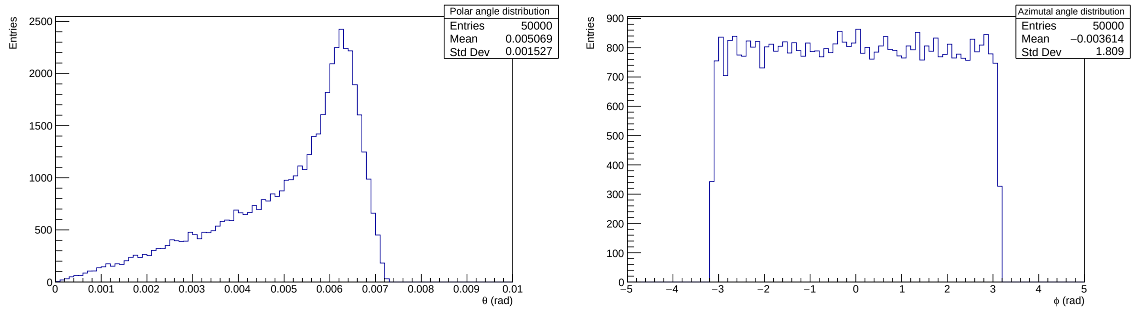

(a) ϕ distribution (b) θ distribution

Figure 4

graph rises and reaches its peak at large angle before rapidly declining. We will revisit this ϕ analysis when we get to section 2.4.

2.4 Correlation Between Muon Energy and Polar Angle

For a setting of pion energy, we need to look at a correlation between muon energy and polar angle. We plot the graph with 6 GeV pion beam and 10% momentum acceptance.

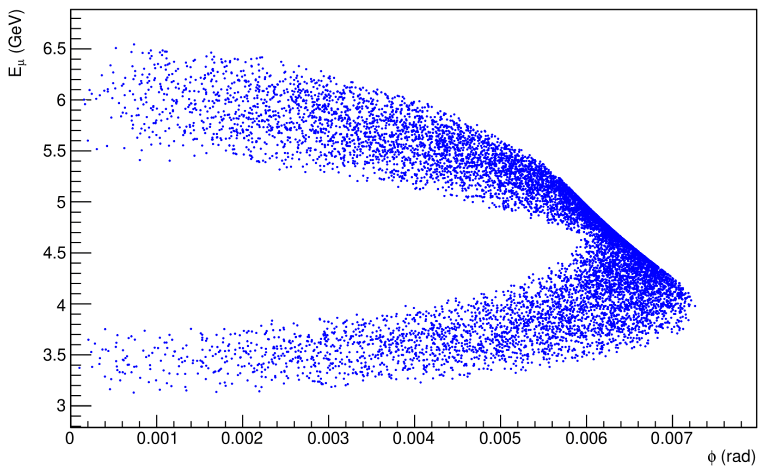

Figure 5: Correlation between muon energy and polar angle

2.4.1 Separation between Forward and Backward Going Muons

In the pion rest frame, if the particles' momentum has a z-component, we can determine which particles go forward or backward by looking at the correlation between energy and polar angle. For example, if the muons align on z-axis, they can have two directions whether forward going or backward going. When we boost to the nuSTORM frame, the forward going muon has the highest energy ,whereas the backward going muon has the lowest energy.

As a result, we have two separated regions in the graph: one above for forward going muons and one below for backward going muons.

2.4.2 The Highest Density Region

Regarding the darkest section in the graph, There are two reasons why it seems to be this way: 1.the p_T distribution as we mentioned in section 2.2 and 2.indistinguishable muons on $x-y$ plane. For the latter, when particles align on the $x-y$ plane and we boost them to z-direction, we cannot distinguish their polar angles and also we cannot separate forward and backward going muons since their momentum has no z-component in the pion rest frame. We can see that this effect reflect in the fig.4a as the highest peak in the graph.

2.5 Effect of Pion Energy on Muon Distribution

We vary energy of the pion beam at 5, 5.5, 6 and 6.5 GeV and plot the graph of energy against polar angle of the muon.

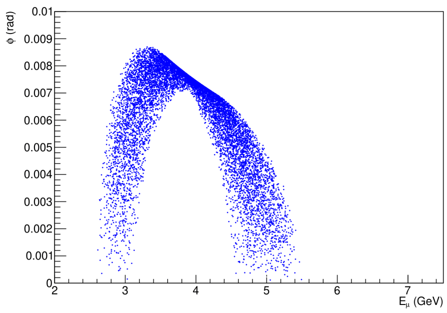

(a) $E_\pi = 5$ GeV

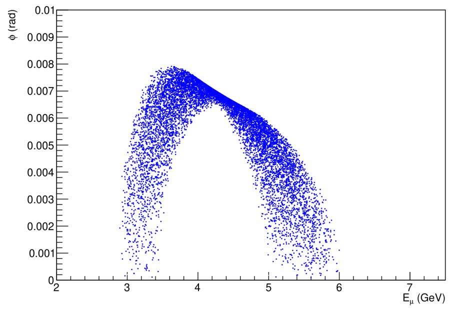

(b) $E_\pi = 5.5$ GeV

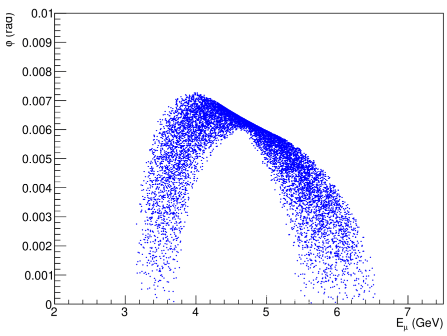

(a) $E_\pi = 6$ GeV

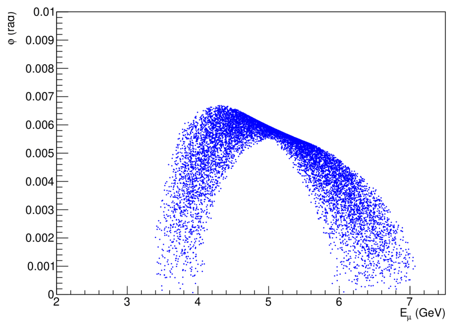

(b) $E_\pi = 6.5$ GeV

As the energy decreases, the plots narrow — there is less boost to distinguish between forward and backward going muons. The peak also dips and rises in angle, indicating that there are less p_z and hence larger angles. As a result, the various energies are stacked on top of each other in a diagonal line.

3 Limiting Phase Space of the Decaying Muons

Not all the particles are produced in a way which allows them to stay within the beam pipe. Muons propagate through the beam pipe with some polar angles. The acceptance of muons entering the beam pipe is determined by their polar angles and decay positions. If particles are close to the edge of the beam pipe, they will hit the beam pipe and disappear. The particles along the way out will be lost unless they are parallel to the beam pipe. Particles in the middle can actually come out to an angle because the focusing magnet in the nuSTORM ring. Even if they are coming out, they will get bent back in : the magnet will keep them in line. Particles are close to the edge, on the other hand, they have less opportunity to be captured before they pass out of the ring. The momentum spectrum of the muons is just the spectrum at decay but we need to produce a spectrum for muons which are captured by the ring (we will present the effect in section 4.1).

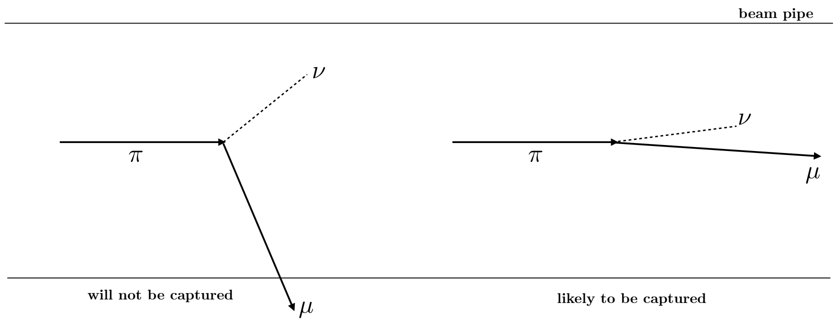

From the paper on Race Track FFAGs studied by Lagrange et al. in [3], Fig 6 is of interest and will allow us to make an estimate of which muons are captured.

3.1 Limiting Functions

For x distribution, we just apply an ellipse equation. However, for y-distribution, we have an asymmetry of the acceptance because the beam is pulled by the magnetic field and is likely to bend left so we need a function of rounded triangle. We can try creating three barrier functions at $2\pi/3$ to get a triangle.

$$\begin{aligned} f(x,y) &= \sum_{i=1}^{3} g\left(-x\cos\theta_i + y\sin\theta_i\right) \\ &= \sum_{i=1}^{3} \left|-x\cos\frac{2\pi i}{3} + y\sin\frac{2\pi i}{3} - \frac{1}{3}\right|^n = 1 \end{aligned} \tag{3.1}$$

Where $g(t) = \left|t - \frac{1}{3}\right|^n$ and $\theta_i = 2\pi\frac{i}{3}$.
The minus sign before x is for flipping the side of the triangle. The shape of this triangle

depends significantly on n. At a low value of n, the shape is almost to be a circle. However, when the n increases, the shape tends to be a triangle: if $n = \infty$, it will be a perfect equilateral triangle. If we generate points inside this function constrained by $f(x, y) < 1$ when $n = 4.5$, we have

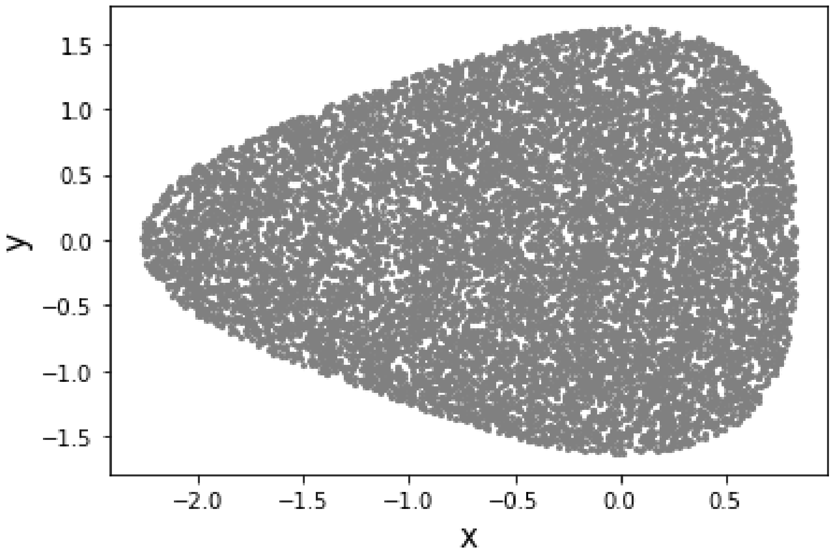

Figure 8: Rounded triangle with $n = 4.5$

We can also generalise the function as

$$f(x, y) = \sum_{i=1}^{3} g\left(\eta(x)_k(x + x_0)\cos\theta_i + \eta(y)_k(y + y_0)\sin\theta_i\right) = 1 \tag{3.2}$$

The $\eta = \pm 1$ stands for flipping the side of the triangle and (x_0, y_0) is the origin point of the triangle.

3.2 Correlation between muon energy and x'(or y')

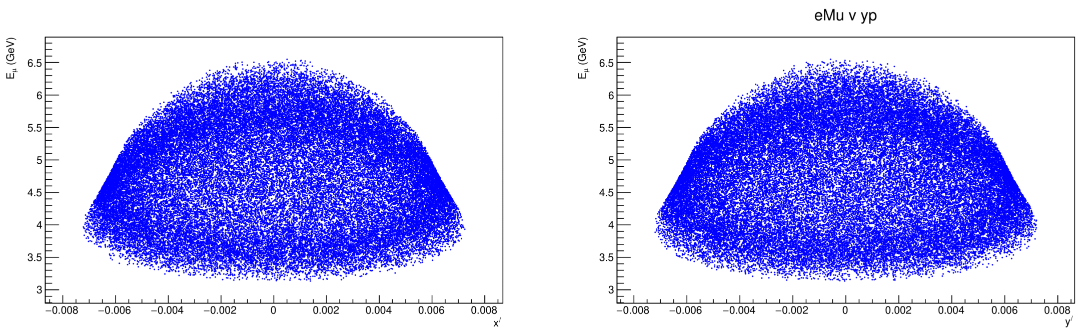

(a) x' distribution

(b) y' distribution

Figure 9: Correlation between muon energy and x'(or y')

Decay contains the values relevant to the muon at the decay point (x, y, z) ,the angle in the x plane p_x/p_z (x'), and the angle in the y plane p_y/p_z (y'). Before we limit the phase space of the muons, we have to look at their correlation with the muon energy. With respect to fig.9a, we can see clearly that the particles are likely to distribute at the edges of the shape with two sides, the upper band for high energy muons and the lower band for low energy muons. In the middle, we have the darker area which is the area when the particles align on $x - y$ plane close to x-axis. However, there is a hole inside this shape with intermediate energies which is the area pertaining to $x - y$ plane that is close to y-axis but distant from x-axis. For the plot of y-distribution, it gives the same shape and the same explanation as the x-distribution.

3.3 Limiting Phase Space at Different Energies

From a wide distribution with a flat top, fig.2b, we get two peaks corresponding to the forward and backward going muons. Intermediate energies are lost sideways. There are more high energy muons because the backward going particles have greater polar angles when we boost to Lab frame and thus less muons are accepted.

Size of the rounded triangle gets smaller as the beam energy decreases since the angle x' or y' get narrower. On the other hand, the size of the triangle gets bigger as the beam energy increases.

3.3.1 $E_\pi = 6$ GeV

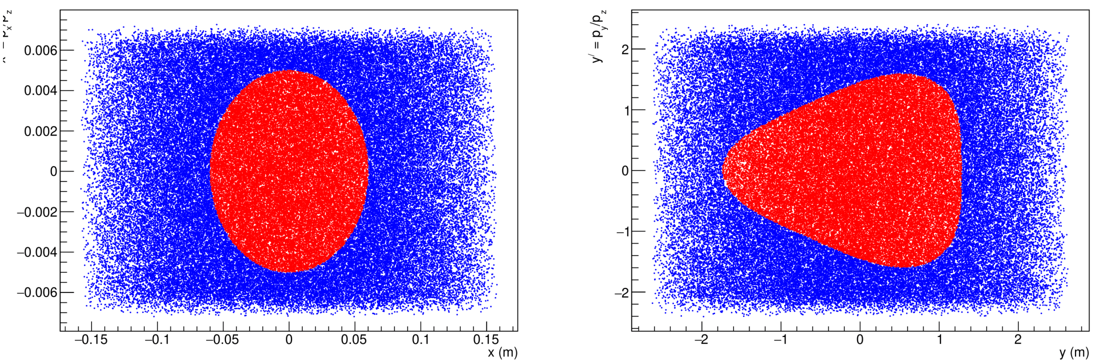

(a) $x' - x$ distribution

(b) $y' - y$ distribution

Figure 10: Limiting phase space of muons

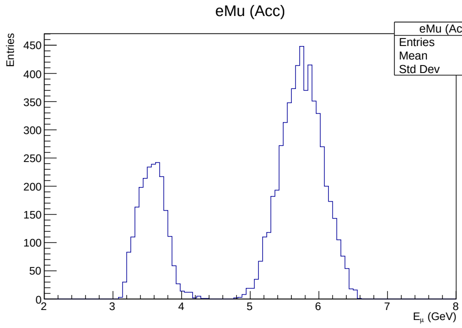

(a) Energy spectrum

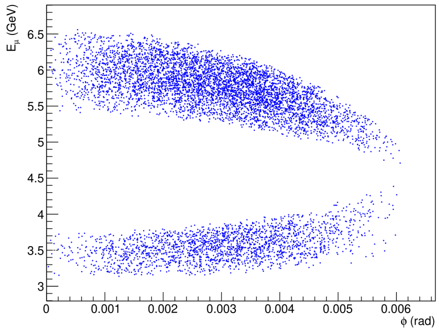

(b) Energy against polar angle

Figure 11: Muons captured by nuSTORM ring

3.3.2 $E_\pi = 2$ GeV

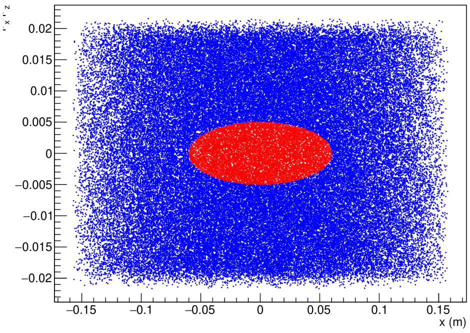

(a) $x' - x$ distribution

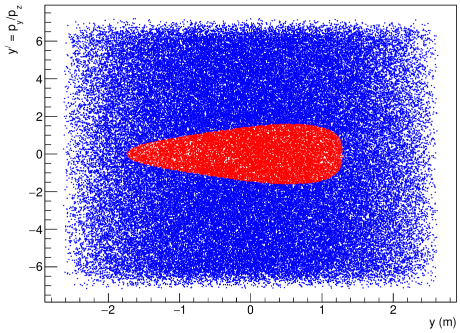

(b) $y' - y$ distribution

Figure 12: Limiting phase space of muons

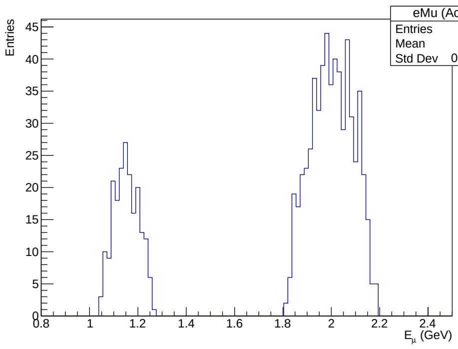

(a) Energy spectrum

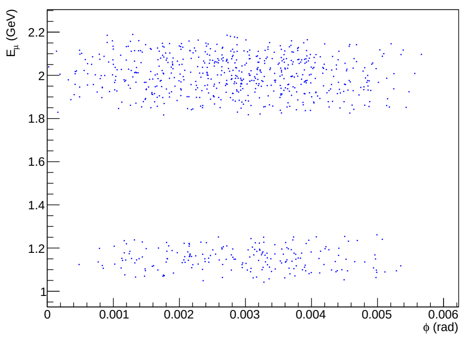

(b) Energy against polar angle

Figure 13: Muons captured by nuSTORM ring

3.3.3 $E_\pi = 8$ GeV

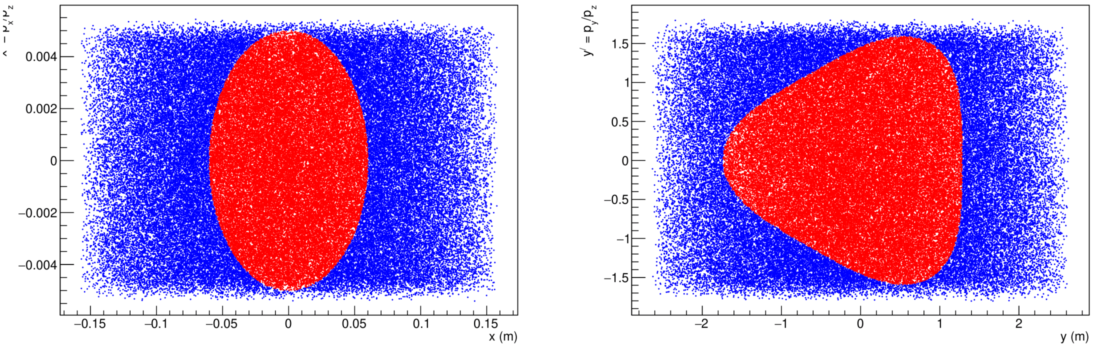

(a) $x' - x$ distribution (b) $y' - y$ distribution

Figure 14: Limiting phase space of muons

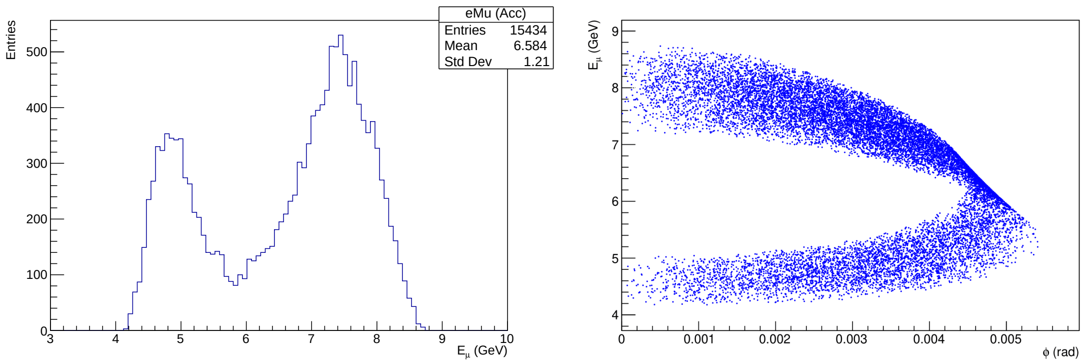

(a) Energy spectrum (b) Energy against polar angle

Figure 15: Muons captured by nuSTORM ring

4 Results

4.1 Muon Spectrum after Limiting Phase Space

Since we have two separated peaks, the top peak for high energy muons is of interest. We fit the top peak with gaussian curve in order to get two parameters, the mean energy and the width σ of the distribution. We approximate the muon yield in the accepted area of the upper peak per the incident pion which will be used to solve the problem of carrying the normalization through the simulation chain in the sequel.

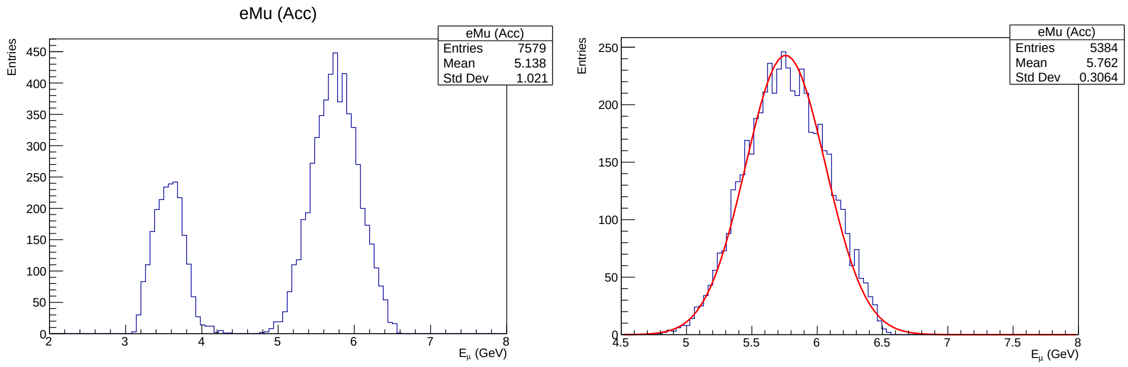

Figure 16: Fitting energy spectrum of the accepted muon of the top peak at 6 GeV pion beam

Table 1: Mean energy, width and efficiency of the muons after limiting their phase space

Pion Energy $\pm$ 10%(GeV)	Muon Energy (GeV) $\pm$ Width(σ) %	eff(%)
1.5	1.51 $\pm$ 4.7%	0.4%
2.0	2.00 $\pm$ 4.9%	0.6%
3.0	2.98 $\pm$ 4.9%	1.2%
4.0	3.94 $\pm$ 4.6%	2.5%
5.0	4.87 $\pm$ 4.8%	5.1%
6.0	5.76 $\pm$ 5.4%	5.4%
6.5	6.18 $\pm$ 5.8%	8.8%
7.0	6.61 $\pm$ 5.9%	11%
7.5	6.97 $\pm$ 6.6%	13%
8.0	7.39 $\pm$ 7.1%	15%

The efficiency goes up because when we are doing relativistic transformation the particles tend to move forward: there are more accepted muons coming down through the beam.

The width of the energy spread on the muon peak is less than the energy spread on the muon. The pion comes in with $\pm$10% and our fit has the maximum at around $\pm$7%. We expect all the forward going particles over the whole 10% to give us beam inside the acceptance. We will come back to solve this subtlety in section 4.4

4.2 Beam Emittance

The evolution of each particle's position in a six-dimensional-space with coordinates (x, p_x, y, p_y, z, p_z) defines the evolution of a particle along the a beamline . The emittance is the main quantity that characterizes the quality of the phase space of the beam. It is a measure of particle coordinates' average spread in position-and-momentum phase space. Moreover, in most of the experiments, phase space emittance is substituted by trace space emittance (also known as geometrical emittance), which is defined in the planes (x, x') and (y, y'), where x' and y' are the transverse angles with respect to the ideal beam trajectory. The trace-space emittance $\varepsilon_{\text{tr,rms}}$ is defined as

$$\varepsilon_{\text{tr,rms}} = \sqrt{\langle x^2 \rangle \langle x'^2 \rangle - \langle xx' \rangle^2} \tag{4.1}$$

Where,

$$\left\langle x^2 \right\rangle = \frac{\sum x^2}{n}, \quad \left\langle x'^2 \right\rangle = \frac{\sum x'^2}{n}, \quad \left\langle xx' \right\rangle \quad = \frac{\sum xx'}{n} \tag{4.2}$$

and all sums are performed for the n particles in the distribution, i.e.,$\sum x = \sum_{i=1}^{n} x_i$.
The Courant-Snyder parameters are closely related to the beam matrix.

$$\begin{bmatrix} \langle x^2 \rangle & \langle xx' \rangle \\ \langle xx' \rangle & \langle x'^2 \rangle \end{bmatrix} = \varepsilon \begin{bmatrix} \beta & -\alpha \\ -\alpha & \gamma \end{bmatrix} \tag{4.3}$$

The beam size depends only on the emittance and the β parameter through the relation $\sigma = \sqrt{\varepsilon\beta}$. We calculate $\varepsilon_{\text{tr,rms}}$ and β of the high energy muon beam with input 6 GeV pion energy.
For the $x - p_x$ plane, we have

$$\begin{aligned} \epsilon_x &= 5.01 \times 10^{-5} \quad \text{m} \cdot \text{rad} \\ \beta_x &= 12.23 \quad \text{m/rad} \end{aligned} \tag{4.4}$$

For the $y - p_y$ plane, we have

$$\begin{aligned} \epsilon_y &= 1.03 \times 10^{-4} \quad \text{m} \cdot \text{rad} \\ \beta_y &= 18.89 \quad \text{m/rad} \end{aligned} \tag{4.5}$$

When we evaluate $\varepsilon_{\text{tr,rms}}$ and β at different energies, they are invariant and do not depend on energy as we expect because the limiting function using in the section 3.1 is momentum independence. Moreover, when we increase the energy by scaling factor η, $E' = \eta E(\eta > 1)$, the x' and y' change into x'/η and y'/η and also the shape of the limiting function is bigger (A $\rightarrow \eta A$), making the emittance invariant.

4.3 Muon Production Rates

We estimate the muon production yield off of the pion beam with different energies with 10% momentum acceptance by using NuMI data [4] for protons-on-target (POT) with organised in bins of p_z and p_T and including normalization in the information.

We use the measured $N(\pi^+)$/POT and $N(\pi^-)$/POT yields from 120 GeV/c proton incident in order to find the pion production rates. We therefore combine the pion production rates and the proportion of the accepted muons from the top peak per pion to get the normalization of the muons captured by the nuSTROM ring with a given number of pions per proton on target. The available pion energies in the NuMI target corresponding to our pion decay are 1, 2, 5, and 7 GeV. So, we will focus at these particular range of energies.

However, the number we got is not an actual number, we still need the full simulation of the whole experiment but it provides us with the initial number and idea of the experiment.

Pion energy (GeV)	$N(\pi)/$**POT**	$N(\mu)/$**POT** (lower bound)	$N(\mu)/$**POT** (centre)	$N(\mu)/$**POT** (upper bound)
1.0 ± 0.1	7.5835e-01	9.59e-04	1.12e-03	1.28e-03
2.0 ± 0.1	7.845e-01	4.11e-03	4.57e-03	4.79e-03
5.0 ± 0.1	3.79e-01	1.33e-02	1.38e-02	1.43e-02
7.0 ± 0.1	2.7258e-01	2.01e-02	2.08e-02	2.13e-02

Table 2: The normalization of the muons captured by the nuSTORM ring with a given number of pions per proton on target.

4.4 The Subtlety of the Energy Spread

In the section 4.1, we fit the histograms with a gaussian curve. But we can actually fit them with parabolic curve, we can see in fig.17b that the energy spread is about 11 percent which is the width we think it ought to be.

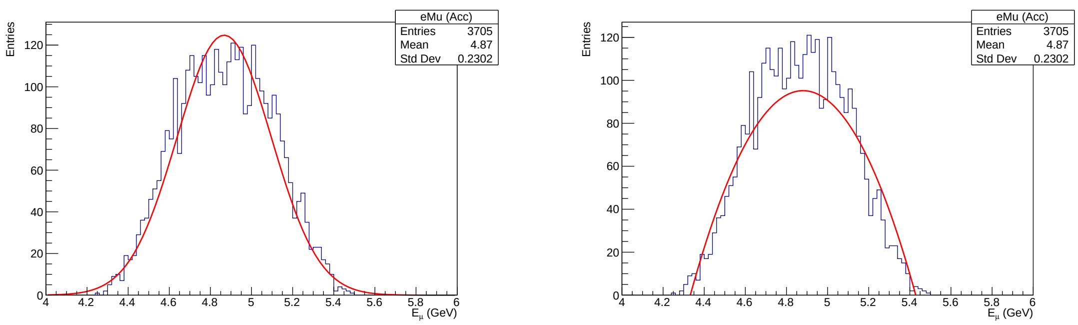

(a) $E_\mu^{\rm Gaus} = 4.87 \pm 4.7\%$GeV

(b) $E_\mu^{\rm Para} = 4.89 \pm 11\%$GeV

Figure 17: Fitting energy spectrum of the top peak at 5 GeV pion beam

We consider high statistic plot (300000 events of the pion decay). It is neither the proper gaussian nor the parabola. Most of them are parabolic but there are some tails which go out a little bit further. So, they should be a combination of gaussian and parabolic curves.

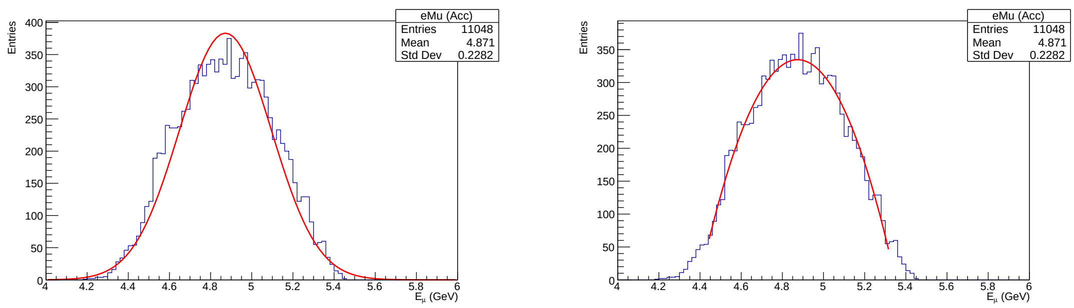

Figure 18: Fitting energy spectrum of the top peak at 5 GeV pion beam

4.5 Neutrino Production Rates

For the muon decay, we simulate by using nuSim with the parabolic muon beam distribution. We fit the muon peaks from the pion decay with parabolic curve and inject them into the simulation to find the normalization of the neutrinos per POT which we summarise in the table below.

Muon energy (GeV)	energy bins (GeV)	$N(e)$ $/N(\mu)$	$N(\nu_\mu)$ $/N(\mu)$	$N(\nu_e)$ $/N(\mu)$	$N(\nu)$ $/N(\mu)$	$N(\nu)$ **/POT**
1.01 ± 10%	[0.00-0.50)	7.21e-01	7.22e-01	8.06e-01	1.53e+00	1.71e-03
1.01 ± 10%	[0.50-1.00)	2.79e-01	2.78e-01	1.94e-01	4.72e-01	5.28e-04
1.01 ± 10%	[1.00-1.50)	1.55e-04	1.40e-04		1.40e-04	1.57e-07
2.00 ± 10%	[0.00-0.50)	4.02e-01	4.02e-01	4.69e-01	8.71e-01	9.76e-04
2.00 ± 10%	[0.50-1.00)	3.28e-01	3.27e-01	3.41e-01	6.68e-01	7.48e-04
2.00 ± 10%	[1.00-1.50)	2.03e-01	2.05e-01	1.61e-01	3.67e-01	4.11e-04
2.00 ± 10%	[1.50-2.00)	6.70e-02	6.60e-02	2.79e-02	9.38e-02	1.05e-04
4.89 ± 11%	[0.00-0.50)	1.70e-01	1.70e-01	2.02e-01	3.71e-01	4.16e-04
4.89 ± 11%	[0.50-1.00)	1.65e-01	1.62e-01	1.92e-01	3.54e-01	3.97e-04
4.89 ± 11%	[1.00-1.50)	1.53e-01	1.52e-01	1.70e-01	3.21e-01	3.60e-04
4.89 ± 11%	[1.50-2.00)	1.37e-01	1.37e-01	1.45e-01	2.83e-01	3.17e-04
4.89 ± 11%	[2.00-2.50)	1.19e-01	1.20e-01	1.14e-01	2.34e-01	2.62e-04
4.89 ± 11%	[2.50-3.00)	9.77e-02	9.69e-02	8.38e-02	1.81e-01	2.02e-04
4.89 ± 11%	[3.00-3.50)	7.42e-02	7.61e-02	5.30e-02	1.29e-01	1.45e-04
4.89 ± 11%	[3.50-4.00)	5.10e-02	5.12e-02	2.88e-02	8.00e-02	8.96e-05
4.89 ± 11%	[4.00-4.50)	2.80e-02	2.85e-02	1.03e-02	3.88e-02	4.34e-05
4.89 ± 11%	[4.50-5.00)	6.64e-03	6.22e-03	1.04e-03	7.26e-03	8.13e-06
6.63 ± 14%	[0.00-0.50)	1.25e-01	1.27e-01	1.49e-01	2.76e-01	3.10e-04
6.63 ± 14%	[0.50-1.00)	1.22e-01	1.22e-01	1.46e-01	2.68e-01	3.01e-04
6.63 ± 14%	[1.00-1.50)	1.18e-01	1.18e-01	1.36e-01	2.53e-01	2.84e-04
6.63 ± 14%	[1.50-2.00)	1.12e-01	1.12e-01	1.23e-01	2.35e-01	2.63e-04
6.63 ± 14%	[2.00-2.50)	1.04e-01	1.03e-01	1.11e-01	2.14e-01	2.40e-04
6.63 ± 14%	[2.50-3.00)	9.37e-02	9.47e-02	9.43e-02	1.89e-01	2.12e-04
6.63 ± 14%	[3.00-3.50)	8.30e-02	8.27e-02	7.91e-02	1.62e-01	1.81e-04
6.63 ± 14%	[3.50-4.00)	7.20e-02	7.11e-02	6.07e-02	1.32e-01	1.48e-04
6.63 ± 14%	[4.00-4.50)	5.88e-02	5.94e-02	4.44e-02	1.04e-01	1.16e-04
6.63 ± 14%	[4.50-5.00)	4.61e-02	4.68e-02	2.93e-02	7.61e-02	8.53e-05
6.63 ± 14%	[5.00-5.50)	3.37e-02	3.31e-02	1.77e-02	5.09e-02	5.70e-05
6.63 ± 14%	[5.50-6.00)	2.10e-02	2.13e-02	7.83e-03	2.91e-02	3.26e-05
6.63 ± 14%	[6.00-6.50)	9.10e-03	8.48e-03	1.63e-03	1.01e-02	1.13e-05
6.63 ± 14%	[6.50-7.00)	5.40e-04	3.75e-04	2.00e-05	3.95e-04	4.42e-07

5 Conclusions

We use the data from nuSim [1] based on the design in [2] and maintained using the GitHub version-control system. We concentrate at the pion decay of nuSTORM production straight. The pion decay into muon and muon-neutrino with 10 % momentum acceptance.
The correlation between energy and polar angle of muons is well organised into three regions. The upper band for high energy particles which are the forward going muons and the lower band for low energy particles which are the backward going muons in the pion rest frame. For the intermediate energy, we have the particles on the $x-y$ plane in the pion rest frame.

We would like to approximate the actual particles captured by the nuSTORM ring through the beam pipe and figure out their properties. Thus, we limit the phase space of the muons with the ellipse for the x-distribution and the rounded triangle for the y-distribution. After we limit phase space, the energy distribution of the accepted muons is separated into two main peaks, the bottom peak for low energy muons and the top peak for high energy muons. The intermediate energy muons are lost sideways. The top peak is of interest. The muon distribution is the combination of gaussian and parabolic distribution as we can see in the section 4.4.

We can approximate the probabilities of getting this muons at particular range of energies per pion. Thus, we can use this number together with the number from NuMI target for the pion production rates per proton in order to get the normalization of the muons. Finally, we integrate this result with the simulation of the muon decay to get the normalization of the neutrinos through the whole simulation chain.

Acknowledgments

I would like to express my gratitude to the European Organization for Nuclear Research (CERN) who organized this Summer Student Programme and CERN Summer Student Team. I would like to thank you my supervisor, Professor Paul Kyberd, for his guidance throughout this project. His availability for questions or a quick chat makes the virtual programme the best experience.

This work is funded from the Thai govern- ment through the Thailand Synchrotron Light Institute, to which I express my deep grati- tude.

References

[1] P. Kyberd and K. Long, "nuSIM: parameters for first simulation of neutrino spectra," Tech. Rep. nuSIM-2021-01, March, 2021. https://www.nustorm.org/trac/raw-attachment/wiki/Software-and-computing/Documentation/2021/nuSIM-doc-01.pdf.

[2] C. Ahdida, R. Appleby, W. Bartmann, J. Bauche, M. Calviani, J. Gall, S. Gilardoni, B. Goddard, C. Hessler, P. Huber, I. Efthymiopoulos, J. Lagrange, M. Lamont, K. Long, J. Osborne, J. Pasternak, F. Soler, S. Tygier, and F. Velotti, "nuSTORM at CERN: Feasibility Study," Tech. Rep. CERN-PBC-REPORT-2019-003, CERN, Geneva, Oct, 2020. http://cds.cern.ch/record/2654649.

[3] J.-B. Lagrange and R.B. Appleby and J.M. Garland and J. Pasternak and S. Tygier, "Racetrack FFAG muon decay ring for nuSTORM with triplet focusing,"arXiv:1806.02172v2 [physics.acc-ph] 3 Sep 2018.

[4] J.M. Paley et al., "Measurement of Charged Pion Production Yields off the NuMI Target," arXiv:404.5882v1 [hep-ex] 23 Apr 2014.

[5] Formaggio, J. A. and Zeller, G. P., "From eV to EeV: Neutrino cross sections across energy scales," arXiv:1305.7513v1 [hep-ex] 31 May 2013.

[6] Barbara Marchetti, "Particle Beam Diagnostics," arXiv:2008.05896v1 [physics.acc-ph] 13 Aug 2020.

CERN

ไทยเซิร์น Siam Photon สวทช NSTDA NARIT สทน TINT สสวท ThEP CENTER กฟผ. POWER OF INNOVATION FOUNDATION